

Modelling the transport and adsorption dynamics of arsenic in a soil bed filter

Raka Mondal^a, Sourav Mondal^a, Krishnasri V. Kurada^b, Saikat Bhattacharjee^b, Sourav Sengupta^b,
Mrinmoy Mondal^b, Sankha Karmakar^b, Sirshendu De^b, Ian M. Griffiths^{a,*}

^aMathematical Institute, University of Oxford, Oxford OX2 6GG, UK

^bDepartment of Chemical Engineering, Indian Institute of Technology Kharagpur, Kharagpur 721302, India

Abstract

Arsenic is among the most hazardous contaminants present in drinking water. Recent increase in agricultural growth and fertiliser use in India and Bangladesh has led to the release of naturally occurring arsenic from the rocks, creating a major public health issue. A novel technology has been developed using naturally abundant laterite soil to filter arsenic, providing potable water to more than 5000 people. To upscale this technology and realise its full potential, a comprehensive understanding of the dependence of filter life on operating regime (flow rate, arsenic concentration and filter size) is essential. We present a mathematical model that characterises arsenic removal, circumventing the need for time-consuming experiments. The model incorporates inter- and intra-particle mass transport within the filter medium. The resulting model enables prediction of a filter lifetime in a specified role, such as on a domestic or community scale, and should assist in future filter deployment and maintenance.

Keywords: arsenic removal; mathematical modelling; computational fluid dynamics; intra-particle dynamics; asymptotic analysis; India and Bangladesh

1. Introduction

The availability of safe drinking water is a necessity for sustainable life. Sources of drinking water, both underground and surface, are extremely susceptible to contamination, from physical, chemical, biological, or radioactive sources [1]. Currently, various water-purification technologies are globally adopted to remove contaminants. There are strict guidelines for safe drinking water, set by concerned agencies, such as the Environmental Protection Agency and the World Health Organization (WHO) that are closely monitored to ensure consumption of safe drinking water.

Arsenic (*As*), a naturally occurring element found in rocks and the earth's crust, is among the most hazardous contaminants in drinking water sources [2]. *As* is embedded in geological sources and enters into the water supply as the rocks are eroded by the flow of water from rivers and rainwater. Further, use of manure containing phosphate and other agricultural activities lead to the break down of arsenic binding bonds in different rocks, releasing *As* into the groundwater. Consequently, if not properly managed, the level of *As* contamination will continue to rise because of human activity and agricultural growth. At present, more than 200 million people and over 70 countries in the world are affected by *As* contamination [3]. A safe limit of 10 $\mu\text{g/L}$ of *As* in drinking water was declared by WHO in 2000 [4, 5]. To address this issue effectively, it is necessary to have a water-purification technology that: (i) meets

*Corresponding author
Preprint submitted to *Chemical Engineering Journal*.
Email address: ian.griffiths@maths.ox.ac.uk (Ian M. Griffiths)

36 the safe drinking-water criteria; (ii) requires minimal energy; (iii) offers high throughput; (iv) is easy to
37 scale up to cater for large population; and (v) generates minimal waste.

38 A novel strategy that achieves all five of these criteria has recently been discovered, using readily available
39 laterite soil [6, 7]. Laterite is iron-rich and is able to remove *As* through adsorption. Raw laterite is
40 treated chemically to enhance the surface area and increase adsorption capacity several fold.

41 However, as with any other adsorption medium, the filter has a certain lifespan, beyond which the filtrate
42 no longer meets the safe limit for drinking water. For the design and successful implementation of this
43 new filtration technology, it is therefore vital to predict the long-term behaviour of this technology.
44 This long-term performance is influenced by the operating conditions, such as the input rate of the
45 contaminated water, the mass of the adsorbent and the contaminant concentration level. Moreover, since
46 the typical lifetime of such filters is of the order of several years, conducting experiments to determine
47 the dependence of filter lifetime on the operating parameters is impractical. This therefore warrants the
48 need of a suitable mathematical model to understand and characterise the operation and to predict the
49 adsorption behaviour and filtration performance.

50 Several studies exist in the literature reporting on the theory of adsorption by different adsorbent media.
51 The kinetics of *As* adsorption in water by raw laterite has been reported using a resistance-in-series
52 model [7]. A shrinking-core model by Maiti et al. [8] was used to calculate the effective pore diffusivity
53 and the external mass-transfer coefficient. Here, the adsorbent is assumed to be composed of spherical
54 particles, around which the fluid flows and the contaminants are adsorbed. The adsorbed species pene-
55 trate into the adsorbent so that the core of unaffected material shrinks with time. A theory to explain
56 the different steps involved in *As* removal from groundwater by adsorption has been reported by Maji et
57 al. [9], determining the interplay of diffusion and adsorption. However, in these works, the kinetics of *As*
58 adsorption was studied under well-stirred batch conditions. Such experiments do not simulate the actual
59 removal performance when contaminated water flows past a stagnant bed of adsorbent particles. Thus,
60 aforementioned models do not predict the long-term performance of an actual filter, in which hydrody-
61 namics also plays a role. Semi-empirical and empirical models are available to quantify the performance
62 of an adsorption bed under continuous operating conditions. However, these models are associated with
63 certain assumptions, thereby limiting their applications. For example, the Adams–Bohart model as-
64 sumes that the adsorption rate is proportional to the residual adsorption capacity and the contaminant
65 concentration [10]. The Wolborska model assumes low fluid velocity through the column and dominance
66 of diffusion over convection [11]. Again, however, none of these models account for the coupling of the
67 fluid flow to the transport of the contaminants, despite its potentially significant role.

68 A key feature of *As* removal by laterite soil is the intra-particle dynamics. *As* is not only removed via
69 surface adsorption onto laterite particles but through penetration into its core and adsorption within
70 the internal pore structure. Employing a conventional adsorption-isotherm model for surface adsorption
71 leads to an anomaly between the predicted and experimentally observed *As* removal rate.

72 In order to circumvent the limitations of semi-empirical and empirical models, in this paper we develop
73 a theory based on first principles to describe the fluid flow through the laterite soil (a porous medium),
74 which is coupled to the convective, diffusive and adsorptive transport for the contaminant. We also

75 account for the transport dynamics within the porous adsorbent particle. The unknown A_s diffusivity in
76 the porous medium as well as the intra-particle diffusion is determined by comparing with the results of
77 simple experiments. The model is then fully specified and is used to predict two defining properties of the
78 filter for any set of physical characteristics of the system, namely the *lifetime* and the *breakthrough time* of
79 the filter. The breakthrough time is defined as the time when the adsorbent bed becomes exhausted with
80 contaminant and loses the capacity for any further adsorption. The lifetime of the filter is the time when
81 the concentration of contaminant in the exit stream reaches the safe limit for the intended purpose, which
82 is reached before breakthrough. Beyond the lifetime, the filter is no longer fit to produce safe drinking
83 water. Knowing the filter lifetime is imperative in the design of a filter unit and is an outcome of the
84 model presented that cannot be estimated convincingly from simple semi-empirical models.
85 In this paper we will develop a theoretical model that predicts the operating lifetime of a filter given the
86 input parameters, namely, the amount of treated laterite in the filter, the required flow rate, and the
87 inlet A_s concentration. The model will be used to explore the adsorption behaviour within the particles,
88 which cannot be assessed experimentally. The main objective of the model will be to use the short-term
89 laboratory-scale experimental data to predict the long-term filtration behaviour and thus the lifetime of
90 a field-scale filter. The model will also provide a predictive tool for upscaling, to determine the filter size
91 required to generate a given flow rate for a given period to supply in a school or local community. At
92 present, more than 20 filters have been deployed for domestic use and three filter assemblies have been
93 established for community use. Predicting the precise lifetime of these filters under the real operating
94 conditions remains a challenge [12]. We will use our model to extract a performance–lifetime relationship
95 for field implementation providing a protocol for ensuring a safe and sustainable operation.

96 2. Mathematical model

97 A typical filter set-up consists of laterite soil housed in a cylindrical container into which the fluid enters
98 uniformly across the top of the filter (see Fig. 1, left). We model the column using a cylindrical coordinate
99 system (r, θ, z) with radial symmetry (Fig. 1, right).

100 The mathematical model comprises three different aspects: flow of the contaminated water through the
101 interstitial space of the porous medium, and transport and adsorption of the contaminant species.

102 2.1. Flow model

103 The flow of incompressible fluid through the porous medium can be described using the continuity and
104 Darcy–Brinkman equations [13]

$$\nabla \cdot \mathbf{u} = 0, \tag{1}$$

$$-\nabla p + \frac{\mu}{\phi} \nabla^2 \mathbf{u} - \frac{\mu \mathbf{u}}{\kappa} = 0. \tag{2}$$

105 Here, $\mathbf{u} = u\mathbf{e}_r + v\mathbf{e}_z$ is the Darcy velocity, with \mathbf{e}_r and \mathbf{e}_z unit vectors in the r and z directions
106 respectively, μ is the dynamic fluid viscosity, p is the fluid pressure and κ and ϕ are the permeability and
107 porosity of the medium, respectively. The Darcy–Brinkman equation governs the flow in a general porous
108 medium for arbitrary flow speeds, and a broad range of porosities and permeabilities, which may also

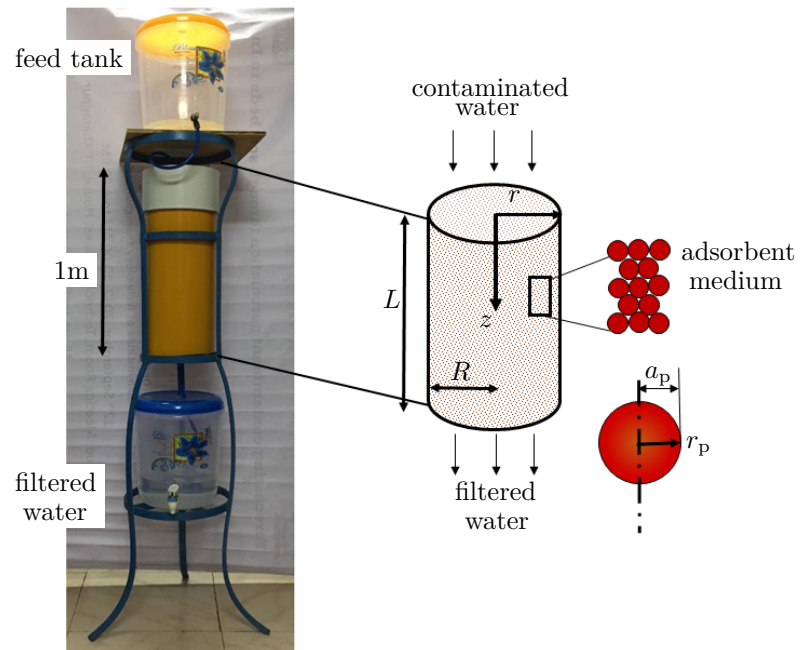


Figure 1: Left: A typical field-scale filter. Contaminated water is held in a feed tank that feeds into a column containing laterite adsorbent material. The filtered water seeps out of the bottom of the column. Right: Schematic of the filtration system. A cylinder of radius R and height L is packed with laterite adsorbent material. The adsorbent material is modelled as porous spheres of radius a_p , which is unchanged by the adsorption of arsenic. We use coordinates (r, z) to denote the position in the filter and r_p to denote the radial position in a particle.

109 vary in space. Later, we will identify dimensionless parameters that determine the relative importance
 110 of the terms. In Eq. (2), the unknown variables \mathbf{u} and p are solved subject to the following initial and
 111 boundary conditions:

- 112 (i) At time $t = 0$, we apply $u = v = 0$ everywhere.
- 113 (ii) The inlet of contaminated water is distributed uniformly over the upper boundary, *i.e.*, $u = 0$ and
 114 $v = v_i$, on $z = 0$ and $0 \leq r \leq R$, where, v_i is a constant inlet velocity of contaminated water.
- 115 (iii) At the filter wall, $r = R$, and $0 \leq z \leq L$, we impose no-slip and no-penetration boundary conditions,
 116 *i.e.*, $u = v = 0$.
- 117 (iv) At the centre, $r = 0$, we apply a symmetry condition, $u = \partial v / \partial r = 0$.
- 118 (v) At the outlet, $z = L$, $0 \leq r \leq R$, the device is open to the atmosphere, so $p = p_a$, which denotes
 119 atmospheric pressure.

120 In practice we expect the second-order term in (2) to be small. However, we choose to retain this here for
 121 generality. In addition, this term will be required to satisfy the no-slip conditions, (iii), that we impose
 122 on the walls of the filter. We therefore expect this term to become important near the boundaries of the
 123 filter device.

124 2.2. Contaminant transport

125 The transport of contaminant occurs on two distinct length scales, namely at the inter-particle and
 126 intra-particle level.

127 2.2.1. Inter-particle transport

128 The contaminant transport is modelled, for dilute concentrations, by the advection–diffusion equation

$$\phi \frac{\partial c}{\partial t} + \mathbf{u} \cdot \nabla c = D_1 \nabla^2 c - k_f \xi (c - c_p |_{r_p=a_p}), \quad (3)$$

129 where $c(r, z, t)$ is the contaminant (*As*) concentration (kg/m^3), D_1 is the effective diffusion coefficient
 130 (constant) of contaminant in the porous bed, k_f is the mass-transfer coefficient at the particle interface,
 131 and $c_p |_{r_p=a_p}$ is the contaminant concentration at the particle surface ; k_f is less easily determined but
 132 may be related to other system properties as we will see later (Eq. (24)). We assume the particles to
 133 be spheres of radius a_p and $r_p \in [0, a_p]$ denotes the radial coordinate for the particle (see Fig. 1 and
 134 following section). The surface area factor exposed to the free fluid of the porous bed (not including
 135 inside the pores), ξ , for randomly packed spherical particles is [14]

$$\xi = \frac{3}{a_p} (1 - \phi). \quad (4)$$

136 Eq. (3) is subjected to the following initial and boundary conditions:

- 137 (i) Initially the filter does not contain any *As*, and so $c = 0$ everywhere at $t = 0$.
- 138 (ii) At the inlet, $z = 0$ and $0 \leq r \leq R$ the contaminant concentration is a constant, $c = c_f$.
- 139 (iii) At the filter wall, $r = R$ and $0 \leq z \leq L$, we apply a no-flux condition, $\partial c / \partial r = 0$.
- 140 (iv) At the centre, $r = 0$, we apply a symmetry condition, $\partial c / \partial r = 0$.
- 141 (v) At the outlet, $z = L$ and $0 \leq r \leq R$, we apply a zero-diffusive-flux condition, $\partial c / \partial z = 0$, so that
 142 contaminant is purely advected out of the filter. This corresponds to a passive boundary condition,
 143 which does not require additional information about what happens once the water exits the filter.

144 *2.2.2. Intra-particle transport*

145 Within a particle, the adsorption–diffusion equation is expressed in the radially symmetric spherical
146 coordinate system as

$$\phi_p \frac{\partial c_p}{\partial t} + (1 - \phi_p) \rho_p \frac{\partial q}{\partial t} = \frac{D_p}{r_p^2} \frac{\partial}{\partial r_p} \left(r_p^2 \frac{\partial c_p}{\partial r_p} \right), \quad (5)$$

147 where c_p is the concentration within the particle, and ϕ_p and ρ_p are the porosity and density of the
148 particles, respectively. The diffusivity of *As* inside the particle is D_p and q is the adsorption capacity
149 (kg per kg of adsorbent). Eq. (5) must be solved at every position (r, z) in the porous domain and so
150 adds an extra lengthscale to the problem.

151 The unknown variables, $c_p(r, r_p, z, t)$ and $q(r, r_p, z, t)$ are solved subject to the following boundary con-
152 ditions for $t > 0$ and initial conditions:

153 (i) At the surface of the particle, $r_p = a_p$, diffusive mass flux from the particle equals the mass flux from
154 the particle to the external medium. Hence, from the flux continuity at $r_p = a_p$,

$$k_f(c - c_p |_{r_p=a_p}) = \phi_p D_p \left. \frac{\partial c_p}{\partial r_p} \right|_{r_p=a_p}, \quad (6)$$

155 for all $0 \leq r \leq R$, $0 \leq z \leq L$.

156 (ii) At the centre of the particle, $r_p = 0$, we apply a symmetry condition, $\partial c_p / \partial r_p = 0$.

157 (iii) Initially the particles do not contain any *As*, so $c_p = 0$ at $t = 0$ for $0 \leq r_p \leq a_p$.

158 To quantify the transient adsorption process, the Langmuir kinetic equation [15] is used,

$$\frac{\partial q}{\partial t} = k_1 c_p (q_m - q) - k_2 q, \quad (7)$$

where $k_{1,2}$ are the adsorption and desorption rate constants, respectively, and q_m is the maximum amount
of contaminant (kg) that can be adsorbed per kg of material. This equation is closed by applying the
initial condition

$$q = 0 \quad \text{at} \quad t = 0. \quad (8)$$

159 Typical parameter values may be found in Table 1.

160 *2.3. Non-dimensionalisation*

We non-dimensionalise the system via the following scalings

$$\begin{aligned} \bar{r} &= \frac{r}{L}, & \bar{r}_p &= \frac{r_p}{a_p}, & \bar{z} &= \frac{z}{L}, & \bar{R} &= \frac{R}{L}, & \bar{t} &= \frac{t D_p}{L^2}, \\ \bar{c} &= \frac{c}{c_f}, & \bar{c}_p &= \frac{c_p}{c_f}, & \bar{q} &= \frac{q}{q_m}, & \bar{\mathbf{u}} &= \mathbf{u}/v_i, & \bar{p} &= p_a + \frac{\kappa}{\mu v_i L} p. \end{aligned} \quad (9)$$

161 The continuity and Darcy–Brinkman equations, Eqs. (1) and (2) become

$$\bar{\nabla} \cdot \bar{\mathbf{u}} = 0, \quad (10)$$

$$-\bar{\nabla} \bar{p} + \frac{Da}{\phi} \bar{\nabla}^2 \bar{\mathbf{u}} - \bar{\mathbf{u}} = 0, \quad (11)$$

where $\bar{\nabla} = \nabla/L$ and

$$Da = \frac{\kappa}{L^2}, \quad (12)$$

Table 1: Properties of the physical variables and system parameters

Properties of the adsorbent	Raw laterite	Treated laterite
Maximum adsorption capacity, q_m (kg/kg)	1.4×10^{-4} [6]	0.0128 [12]
Forward rate constant, k_1 ($\text{m}^3/\text{kg}\cdot\text{s}$)	2.21×10^{-2}	1.44×10^{-5}
Backward rate constant, k_2 (1/s)	3.12×10^{-6}	1.23×10^{-6}
Average density of adsorbent, ρ_p (kg/m^3)	1325 [6]	1050 [12]
Average particle radius, a_p (mm)	2.5 [6]	0.25 [12]
Permeability of adsorbent bed, κ (m^2)	2.9×10^{-8}	1.4×10^{-8}
Average bed porosity, ϕ	0.48 [6]	0.32 [12]
Particle porosity, ϕ_p	0.03 [6]	0.39 [12]
Diffusivity of As through the medium and theoretical prediction from Section 4.1 (m^2/s)	$D_{l,RL}$ 3.7×10^{-10}	$D_{l,TL}$ 2.7×10^{-11}
Diffusivity of As inside the adsorbent particle and theoretical prediction from Section 4.1 (m^2/s)	$D_{p,RL}$ 9.2×10^{-10}	$D_{p,TL}$ 1.4×10^{-10}
Properties of the liquid	Value	
Density of liquid, ρ_l (kg/m^3)	1000	
Viscosity of contaminated water, μ (Pa.s)	8.94×10^{-4}	
Temperature ($^\circ\text{C}$)	25	

162 is the Darcy number for the flow. For the set-ups of interest, $Da = O(10^{-7})$ (see Tables 2 and 3). As
 163 noted earlier, this means that the second-order term in (11) will be small except in a small boundary
 164 layer near the filter walls where the flow field changes to satisfy the no-slip condition.

The dimensionless boundary domains are $\bar{r} \in [0, \bar{R}]$ and $\bar{z} \in [0, 1]$. The dimensionless boundary conditions
 for $t > 0$ and initial conditions for the flow are

$$\bar{u} = 0 \text{ and } \bar{v} = 1, \quad \text{at } \bar{z} = 0, \quad (13a)$$

$$\bar{u} = \bar{v} = 0, \quad \text{at } \bar{r} = \bar{R}, \quad (13b)$$

$$\bar{u} = \frac{\partial \bar{v}}{\partial \bar{r}} = 0, \quad \text{at } \bar{r} = 0, \quad (13c)$$

$$\bar{p} = 0, \quad \text{at } \bar{z} = 1, \quad (13d)$$

$$\bar{u} = \bar{v} = 0, \quad \text{at } \bar{t} = 0. \quad (13e)$$

165 The dimensionless form of Eq. (3) becomes

$$\frac{\alpha}{Pe} \frac{\partial \bar{c}}{\partial \bar{t}} + \bar{u} \frac{\partial \bar{c}}{\partial \bar{r}} + \bar{v} \frac{\partial \bar{c}}{\partial \bar{z}} = \frac{1}{Pe} \left(\frac{\partial^2 \bar{c}}{\partial \bar{z}^2} + \frac{1}{\bar{r}} \frac{\partial}{\partial \bar{r}} \left(\bar{r} \frac{\partial \bar{c}}{\partial \bar{r}} \right) \right) - \mathcal{A}(\bar{c} - \bar{c}_p |_{\bar{r}_p=1}), \quad (14)$$

where

$$Pe = \frac{v_i L}{D_l}, \quad (15)$$

$$\alpha = \phi \frac{D_p}{D_l}, \quad (16)$$

$$\mathcal{A} = \frac{3k_f(1-\phi)L}{v_i a_p} = \frac{3k_f M}{Q_i \rho_p a_p}, \quad (17)$$

Table 2: Typical system properties of the bed in the lab-scale experiments.

System properties	Value
Average inlet concentration of As , c_f ($\mu\text{g/L}$)	80
Average volumetric inflow rate, Q_0 (L/day)	40
Linear inflow rate, v_i (m/s)	3.044×10^{-4}
Filter radius, R (m)	0.022
Filter length, L (m)	0.20

System properties	Experiment 1	Experiment 2	Experiment 3
Material used	RL	TL	RL (0.1m) on top of TL (0.1m)
Re	68.1	68.1	68.1 (for both layers)
Re_p	0.85	0.085	0.85 (top), 0.085 (bottom)
Pe	1.64×10^5	2.25×10^6	1.64×10^5 (top), 2.25×10^6 (bottom)
Da	7.25×10^{-7}	3.5×10^{-7}	7.25×10^{-7} (top), 3.5×10^{-7} (bottom)
Sc_p	0.97×10^3	6.38×10^3	0.97×10^3 (top), 6.38×10^3 (bottom)
Sh	8.1	4.7	8.1 (top), 4.7 (bottom)
β_1	76.9	0.33	76.9 (top layer, RL), 0.33 (bottom)
β_2	135.8	374	135.8 (top), 374 (bottom)
\mathcal{A}	6.40	12.4	6.40 (top), 12.4 (bottom)
\mathcal{B}	0.36	0.26	0.36 (top), 0.26 (bottom)

166 and the mass of adsorbent, $M = \pi R^2 L \rho_p (1 - \phi)$ and $Q_i = \pi R^2 v_i$ is the volumetric inlet flux. The
167 parameter Pe is the Péclet number and is typically large ($O(10^5 - 10^6)$) (see Tables 2 and 3); \mathcal{A} relates
168 the competition between the macroscale convection and intra-particle dynamics. Here, $\mathcal{A} = 6.4 - 12.4$ as
169 reported in Tables 2 and 3, meaning that both the macroscale and microscale phenomena are important,
170 necessitating analysis at both the scales.

171 The associated dimensionless initial and boundary conditions are

$$\bar{c} = 0, \quad \text{at } \bar{t} = 0, \quad (18a)$$

$$\bar{c} = 1, \quad \text{at } \bar{z} = 0, \quad (18b)$$

$$\frac{\partial \bar{c}}{\partial \bar{r}} = 1, \quad \text{at } \bar{r} = \bar{R}, \quad (18c)$$

$$\frac{\partial \bar{c}}{\partial \bar{r}} = 0, \quad \text{at } \bar{r} = 0, \quad (18d)$$

$$\frac{\partial \bar{c}}{\partial \bar{z}} = 1, \quad \text{at } \bar{z} = 1. \quad (18e)$$

172 Since $Pe \gg \mathcal{A}$ and α is also expected to be $O(1)$, the transient term in Eq. (14) can be neglected, to give

$$\bar{u} \frac{\partial \bar{c}}{\partial \bar{r}} + \bar{v} \frac{\partial \bar{c}}{\partial \bar{z}} = \frac{1}{Pe} \left(\frac{\partial^2 \bar{c}}{\partial \bar{z}^2} + \frac{1}{\bar{r}} \frac{\partial}{\partial \bar{r}} \left(\bar{r} \frac{\partial \bar{c}}{\partial \bar{r}} \right) \right) - \mathcal{A} \left(\bar{c} - \bar{c}_p \Big|_{\bar{r}=1} \right). \quad (19)$$

173 There will be a short transient start-up period that will not be captured by this simplified system. We
174 note that in the bulk we would also expect the diffusive terms that are premultiplied by $1/Pe$ to be
175 negligible too, further simplifying this equation, but these will become important near the boundaries

Table 3: Typical system properties for the field-scale experiments composed of TL as the active As removal material.

System properties	Value
Inlet concentration of As, c_f ($\mu\text{g/L}$)	100
Volumetric inflow rate, Q_0 (L/day)	100
Linear inflow rate, v_i (m/s)	3.68×10^{-5}
Radius, R (m)	0.10
Length of laterite region, L (m)	0.35
Length of the whole filter (m)	1.0
Re	14.42
Re_p	0.01
Pe	4.77×10^5
Da	1.14×10^{-7}
Sh	2.94
β_1	1.26
β_2	1145.5
\mathcal{A}	22.0
\mathcal{B}	0.068

176 and are required to satisfy the boundary conditions here, which must be satisfied for all time and so we
 177 retain them for our numerical computation.

178 The dimensionless version of the intra-particle dynamic equation, (Eq. 5), is

$$\left(\frac{a_p}{L}\right)^2 \phi_p \frac{\partial \bar{c}_p}{\partial \bar{t}} + (1 - \phi_p) \mathcal{B} \frac{\partial \bar{q}}{\partial \bar{t}} = \frac{1}{\bar{r}_p^2} \frac{\partial}{\partial \bar{r}_p} \left(\bar{r}_p^2 \frac{\partial \bar{c}_p}{\partial \bar{r}_p} \right) \quad (20)$$

where

$$\mathcal{B} = \frac{\rho_p a_p^2 q_m}{c_f L^2}, \quad (21)$$

179 which quantifies the ratio of intraparticle diffusion to adsorption. In this set-up, $\mathcal{B} = 0.26 - 0.36$, as
 180 observed from Tables 2 and 3. This signifies that these two intra-particle phenomena are comparable
 181 and are important and emphasises the need to study the full-scale intra-particle dynamics.

182 Since, $a_p/L \ll 1$ (see Tables 1 and 2), the temporal term $\partial \bar{c}_p / \partial \bar{t}$ in Eq. (20) can be ignored, leaving

$$(1 - \phi_p) \mathcal{B} \frac{\partial \bar{q}}{\partial \bar{t}} = \frac{1}{\bar{r}_p^2} \frac{\partial}{\partial \bar{r}_p} \left(\bar{r}_p^2 \frac{\partial \bar{c}_p}{\partial \bar{r}_p} \right). \quad (22)$$

183 The dimensionless boundary and initial conditions are

$$Sh(\bar{c} - \bar{c}_p |_{\bar{r}_p=1}) = \phi_p \frac{\partial \bar{c}_p}{\partial \bar{r}_p}, \quad \text{at } \bar{r}_p = 1, \quad (23a)$$

$$\frac{\partial \bar{c}_p}{\partial \bar{r}_p} = 0, \quad \text{at } \bar{r}_p = 0, \quad (23b)$$

$$\bar{c}_p = 0, \quad \text{at } \bar{t} = 0, \quad (23c)$$

184 where $Sh = k_f a_p / D_p = f(Re_p, Sc_p)$ is the Sherwood number. For suitably low flow rates (when the
 185 Reynolds number, $Re = \rho_1 v_i L / \mu \leq 250$, where ρ_1 is the fluid density, which is true in our case as seen in

186 Table 2) around small spherical particles (of around a few mm or smaller), the mass-transfer coefficient
 187 (in terms of Sh) may be expressed in terms of known variables as [16]

$$Sh = 2 + 0.5Re_p^{1/2}Sc_p^{1/3}, \quad (24)$$

188 where $Re_p = \rho_1 v_i a_p / \mu$ and $Sc_p = \mu / \rho_1 D_p$ are the particle Reynolds number and Schmidt number,
 189 respectively. For larger particles other relationships of similar form have been established – see, for
 190 example, [17].) The parameter \mathcal{A} defined in Eq. (17) may be expressed in terms of Sh rather than k_f as
 191 $\mathcal{A} = 3ShD_p(1 - \phi)L/a_p^2 v_i$, which, combined with Eq. (24) allows us to determine \mathcal{A} . The adsorption-
 192 kinetic equation, Eq. (7), is scaled as

$$\frac{\partial \bar{q}}{\partial \bar{t}} = \beta_1 \bar{c}_p(1 - \bar{q}) - \beta_2 \bar{q}, \quad (25)$$

where $\beta_1 = k_1 c_f L^2 / D_p$ and $\beta_2 = k_2 L^2 / D_p$ are the dimensionless adsorption and desorption rates, while
 the initial condition (8) becomes

$$\bar{q} = 0 \quad \text{at} \quad \bar{t} = 0, \quad (26)$$

193 to close the system. Eq. (19) is coupled with the intra-particle mass transport through Eq. (22) at all
 194 (r, z) and the hydrodynamics through Eqs. (10) and (11), all of which are solved together using the
 195 appropriate initial and boundary conditions.

196 2.4. Quantity of interest

The principal quantity of interest is the average concentration of the contaminant at the outlet,

$$\bar{c}_{\text{avg}}(\bar{t}) = \frac{2}{R^2} \int_0^{\bar{R}} \bar{r} \bar{c}|_{\bar{z}=1} d\bar{r}. \quad (27)$$

197 During filtration, eventually the soil bed reaches its maximum adsorption capacity, termed *breakthrough*.
 198 Then, the concentration at the outlet is equal to the concentration at the inlet. Mathematically this
 199 is equivalent to the time at which $\bar{c}(\bar{r}, \bar{z}, \bar{t}) = 1$ everywhere in the filter, at which point the filter is
 200 completely saturated (or exhausted).

201 3. Materials and methods

202 3.1. Laterite material

203 Laterite is a type of soil rich in iron, silica and aluminium found abundantly in hot and wet tropical
 204 areas. The quality of the laterite soil as adsorbent for arsenic can be quantified by degree of laterization
 205 defined as the silica-sesquioxide (S-S) ratio [18]. The smaller the S-S ratio, the higher is the degree of
 206 laterization. The laterite used in this work was taken from Kharagpur (22.346°N, 87.2320°S) having an
 207 S-S ratio of 0.42.

208 Raw laterite is treated with hydrochloric acid (6N) in the ratio 50 g laterite to 200 ml of acid at 70°C
 209 for 2 hours followed by the addition of 4N sodium hydroxide continuously until the pH reached 8.5.
 210 The acid-alkali treatment was carried out under continuous stirring (500 rpm) after which the treated
 211 material was washed using tap water until pH of the wash water reached 6.5 ± 0.5 and was air dried [8].

212 3.2. Adsorption isotherm

213 The adsorption isotherm for the soil-bed material, given by the steady-state version of Eq. (7), was mea-
214 sured by conducting batch experiments with either raw laterite (RL) or treated laterite (TL). Synthetic
215 solutions of As in water with concentrations ranging from 10 mg/L to 1000 mg/L were prepared using
216 sodium arsenate heptahydrate. A fixed quantity of the adsorbent was inserted in a known volume V
217 of synthetic solution and placed in a shaker (speed: 150 rpm temperature: 25 °C). After 24 hours, the
218 adsorbent was filtered and the residual concentration of As was measured using an atomic adsorption
219 spectrophotometer (Analyst 700 coupled with MHS-15, PerkinElmer Instruments, USA). The amount of
220 As adsorbed, q_e , was then calculated using a standardised method employing the dimensional equation
221 expressing conservation of mass:

$$q_e = \frac{(c_0 - c_e)V}{M}, \quad (28)$$

222 where c_0 and c_e are the initial and equilibrium concentrations of arsenic and recall that M denotes the
223 mass of the adsorbent used. This expression was inserted into the Langmuir isotherm, obtained from
224 the steady-state version of Eq. (7), and expressed in linear form,

$$\frac{c_e}{q_e} = \frac{1}{q_m} c_e + \frac{1}{K_0 q_m}, \quad (29)$$

225 where $K_0 = k_1/k_2$ is the adsorption equilibrium constant. Comparing the linear plot with the data
226 allows us to extract the value for q_m (through the gradient) and K_0 (through the intercept), with values
227 given in Table 1.

228 3.3. Kinetic study

The constant k_1 that appears in Eq. (7) was determined by conducting adsorption experiments using a
feed solution of volume V and adsorbent of mass M using a fixed arsenic concentration of 100 mg/L in
the feed. Assuming the concentration in the filter, c , was constant throughout, this was related to the
total adsorbed amount via the mass-balance relationship

$$q = \frac{(c_0 - c)V}{M}. \quad (30)$$

229 Rearranging Eq. (30) for c and inserting into Eq. (7) gives the expression

$$\frac{\partial q}{\partial t} = k_1 \left(c_0 q_m - c_0 q - \frac{q_m q M}{V} + \frac{M q^2}{V} - \frac{q}{K_0} \right). \quad (31)$$

230 Plotting the experimental values for the left-hand side of (31) versus the bracketed term on the right-
231 hand side determines k_1 as the corresponding gradient; k_2 is then determined from $K_0 = k_1/k_2$, with
232 values given in Table 1.

233 3.4. Measurement of bed permeability

234 The properties of the adsorbent bed in the experimental set-up are provided in Table 1. The bed
235 permeability, κ (m^2), was measured by passing distilled water through the bed in the upward direction
236 at varying flow rates Q (from 1 to 20 L/h). The flow rate was controlled by using a regulated DC power
237 supply (Aplab, model: L1602) for the pump; the error is within 2%. The pressure drop across the

238 bed, Δp , was measured using a mercury manometer and plotted against the corresponding flow rate.
239 The permeability was then extracted using Darcy’s law, which follows from Eq. (2) for a unidirectional
240 spatially uniform velocity,

$$\frac{Q}{A} = -\frac{\kappa \Delta p}{\mu L}, \quad (32)$$

241 where $A = \pi R^2$ is the cross-sectional area of the filter, μ is the viscosity of water and L is the column
242 length. The value found for the permeability κ is given in Table 1.

243 3.5. Column studies

244 For the lab-scale study, a cylindrical column of inner radius 0.022 m was used with a wire mesh at
245 the bottom to prevent loss of adsorbent. An overhead tank was filled with synthetic solution of As
246 of a specified concentration and the flow rate was adjusted according to the requirements. The flow
247 rate was controlled using a pinch-cock to get the desired throughput, which is reasonably accurate
248 having a variation of $\pm 5\%$ of the mean value. The flow rate is monitored almost every 6 hours to
249 check for the variability from its preset value. The valve (pinch-cock) opening is adjusted accordingly
250 to ensure the desired flow rate as required. The feed and permeate samples were analysed using an
251 atomic absorption spectrophotometer. Different experiments were conducted varying the feed flow rates,
252 feed As concentration and the bed height. The specifications of the column study along with operating
253 conditions are presented in Table 2.

254 4. Model validation

255 There are two filters of interest: *lab-scale filters* and *field-scale filters*. Lab-scale filters are used to study
256 the system behaviour in a controlled environment; field-scale filters are used in practical scenarios to
257 supply drinking water domestically, in schools, or in communities, and hence they are typically larger
258 (see Table 3). Field-scale filters also consist of layers of different porous materials, each designed to
259 remove a specific contaminant. The TL section of a field-scale filter occupies around 0.35 m of the entire
260 filter height of around 1 m, with the remaining layers having no As adsorption capacity. A photograph of
261 the field-scale filter is shown in Fig. 1 while the lab-scale filter is shown in Fig. 2. The typical dimensions
262 of these filters are presented in Table 2.

263 We first determine the diffusion coefficients (D_1 and D_p) and validate our model with two different
264 experiments using RL and TL as the adsorbent, referred to as experiments 1 and 2 respectively in Table 2.
265 All system parameters are then known. The model is then used to predict the filter performance under
266 varying operating conditions and is compared with the experimental results. Following the validation,
267 the model is used to probe the inter- and intra-particle dynamics that cannot be extracted from the
268 experiments (Sections 5.1 and 5.2). Finally, the model is used to predict the lifetime of the field unit
269 and how it may be used as a tool for determining the required filter for a given challenge. This is the
270 main purpose, allowing predictions to be made that would take many years to find experimentally.

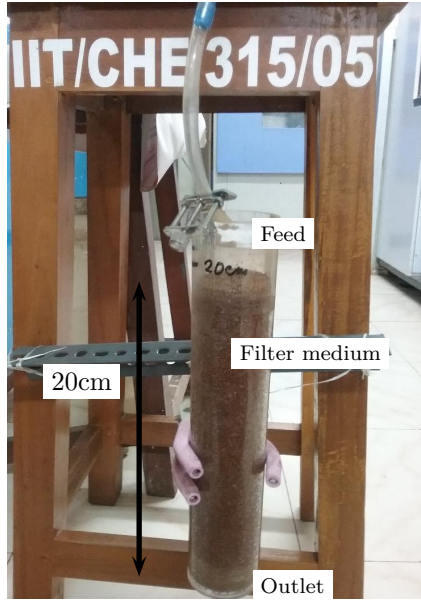


Figure 2: Photograph of a lab-scale filter.

271 *4.1. Parameter estimation*

272 We solve the system of equations (10), (11), (19), (22) and (25), subject to the initial and boundary
 273 conditions (13), (18), (23) and (26) with the dimensionless relation (24), using the finite-element method
 274 package COMSOL v5.4[®] for the values listed in Tables 1 and 2.

275 A synthetic solution of *As* with concentration $80 \mu\text{g/L}$ was introduced into the lab-scale filter at a flow
 276 rate of 40 L/day ($v_i = 3.044 \times 10^{-4} \text{ m/s}$). The diffusion coefficients, D_l and D_p were then determined by
 277 fitting the model to the experimental measurements for \bar{c}_{avg} at the filter outlet for a single-layer lab-scale
 278 filter using least-squares fitting (see Figs. 3a and b).

279 The goodness of fit was verified using the linear regression coefficient, \mathcal{R}^2 , with strong correlation values
 280 of 0.97 for RL and 0.98 for TL [19]. The result of this comparison gives $D_{l,\text{RL}} = 3.7 \times 10^{-10} \text{ m}^2/\text{s}$,
 281 $D_{p,\text{RL}} = 9.2 \times 10^{-10} \text{ m}^2/\text{s}$ for RL, while $D_{l,\text{TL}} = 2.7 \times 10^{-11} \text{ m}^2/\text{s}$, $D_{p,\text{TL}} = 1.4 \times 10^{-10} \text{ m}^2/\text{s}$ are
 282 obtained for TL. We attribute the lower diffusivity in the treated laterite than in the raw laterite to
 283 the lower porosity, which impedes the spread of *As*. Within the pores themselves, the *As* has a much
 284 lower diffusivity in the treated laterite than the raw laterite despite having a much higher porosity, which
 285 has been reported elsewhere [20]. This is thought to be due to the channeling structure within the raw
 286 laterite pore, which increases the mean free path.

287 With the parameters D_l and D_p determined all system parameters are now known and the model can be
 288 used in a fully predictive manner to determine the behaviour in other scenarios. To verify the predictive
 289 power of the model, a series of further simulations were conducted and compared with experimental
 290 data. First, the filtration behaviour of a filter having a single layer of volumes of RL followed by TL,
 291 each occupying a height of $L/2$ was considered (Fig. 3c). In this case, no fitting parameters remained.
 292 The \mathcal{R}^2 value for this system was 0.973, indicating that the model captures the data well. The effect of
 293 varying the feed flow rate, contaminant concentration, and bed height was then studied (Fig. 4) and all
 294 exhibited a good fit. This confirms that the model suitably represents the working system and can be

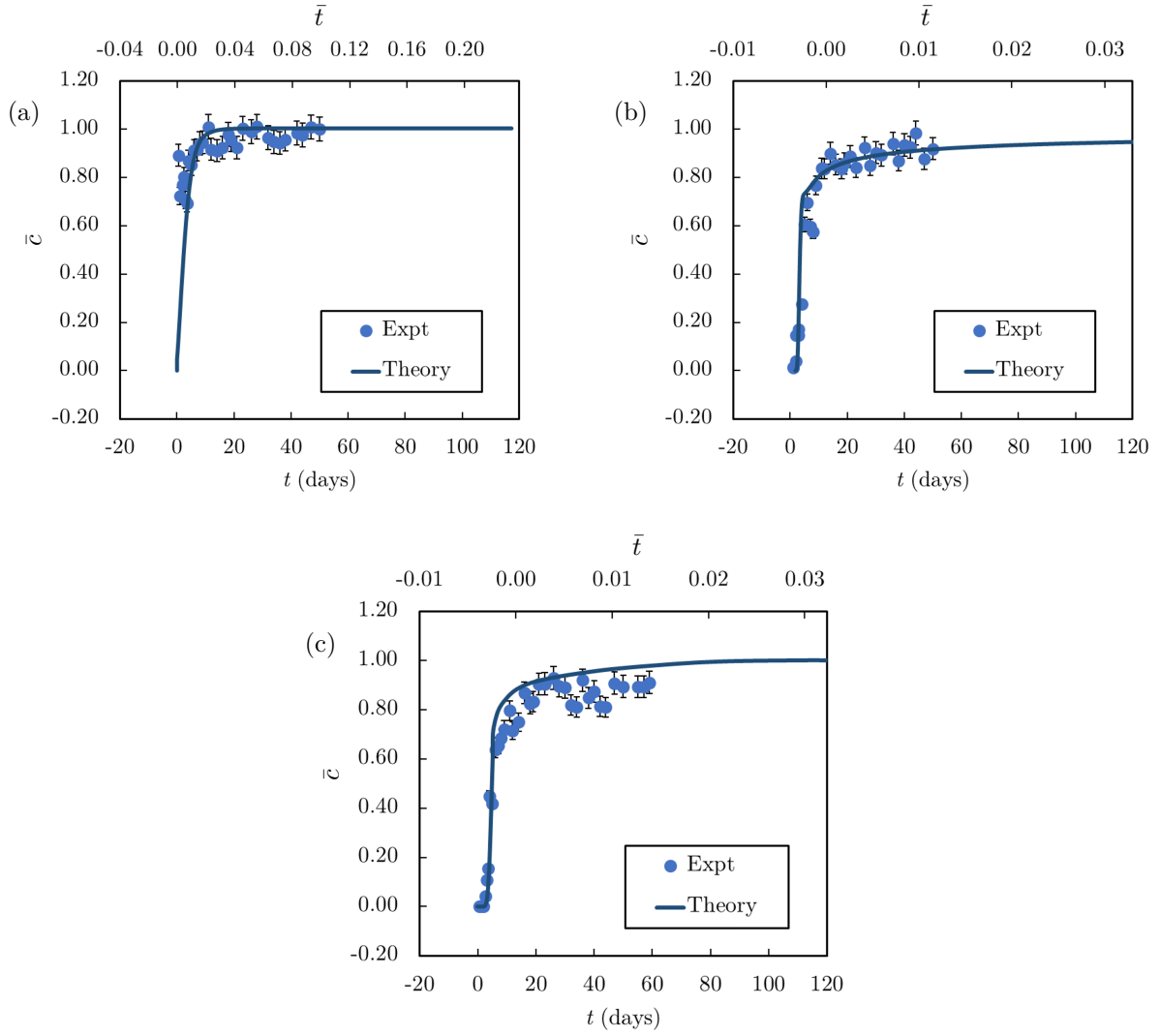


Figure 3: Comparison of the experimental observation with the model simulation using (a) RL as the adsorbent (experiment 1 in Table 2); (b) TL as the adsorbent (experiment 2 in Table 2) and (c) a dual-layer bed of RL (0.1m) followed by TL bed of 0.1m (experiment 3 in Table 2). No fitting parameters are used in (c), supporting the validity of the model. The system conditions are listed in Tables 1 and 2. The error bars represent $\pm 5\%$ of the mean experimental value.

295 taken forward as a predictive tool.

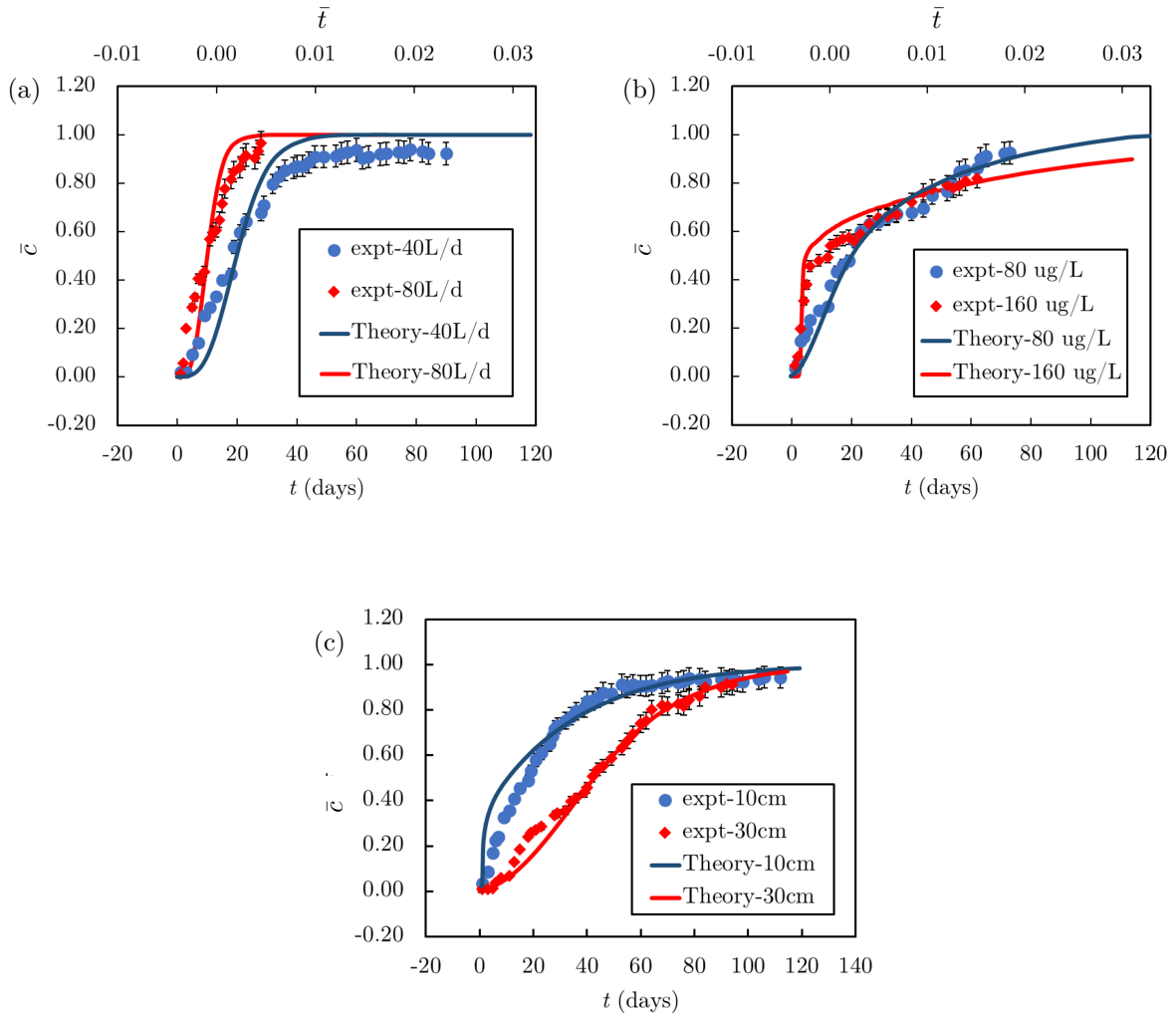


Figure 4: Effect of changing the system conditions on the breakthrough profiles. Variation in (a) the feed flow rate as 40 and 80 L/d, (b) the feed As concentration as 80 and 160 $\mu\text{g/L}$, and (c) the bed height as 10 and 30 cm. The symbols represent the experimental data while the solid line is the model prediction. The error bars represent $\pm 5\%$ of the mean values obtained experimentally. The values of the remaining parameters for the experimental condition and the model calculations are listed in Tables 1 and 2. The dimensionless scale for time is shown on the upper x -axis in (a) and (b). Since the dimensionless time depends on bed height this differs for the two curves displayed in (c) and so is not shown in this graph.

296 5. Model analysis

297 In this section we now use the model to probe the system behaviour more deeply. Specifically, we first
 298 explore the inter and intra-particle dynamics in Sections 5.1 and 5.2 respectively. We then turn our
 299 attention to the key challenge of using our model in a predictive way to determine the lifetime of the
 300 filter and its dependence on the filter parameters in Section 5.3.

301 *5.1. Inter-particle dynamics*

302 The fluid is injected at the top of the filter and the flow is expected to become unidirectional after a
 303 short transient period. Assuming $\bar{\mathbf{u}} = \bar{v}(\bar{r}, \bar{z}, \bar{t})\mathbf{e}_z$, Eq. (10) immediately indicates that \bar{v} is independent
 304 of \bar{z} . The radial component of Eq. (11) then gives $\bar{p} = \bar{p}(\bar{z}, \bar{t})$, while the axial component reads

$$-\frac{\partial \bar{p}}{\partial \bar{z}} + \frac{Da}{\phi \bar{r}} \frac{\partial}{\partial \bar{r}} \left(\bar{r} \frac{\partial \bar{v}}{\partial \bar{r}} \right) - \bar{v} = 0. \quad (33)$$

305 Eq. (33) possesses an analytic solution, which, upon application of the symmetry boundary conditions
 306 $\partial \bar{v} / \partial \bar{r} = 0$ on $\bar{r} = 0$ and the no-slip condition $\bar{v} = 0$ on $\bar{r} = \bar{R}$, gives

$$\bar{v} = \left[\frac{I_0 \left(\sqrt{\frac{\phi}{Da}} \bar{r} \right)}{I_0 \left(\sqrt{\frac{\phi}{Da}} \bar{R} \right)} - 1 \right] \frac{\partial \bar{p}}{\partial \bar{z}}, \quad (34)$$

307 where I_n denotes the modified Bessel function of the first kind, with $n = 0$ in this case. Application of
 308 the dimensionless inlet flux condition in integrated form,

$$\int_0^{\bar{R}} \bar{r} \bar{v} \, d\bar{r} = \frac{1}{2} \bar{R}^2, \quad (35)$$

309 provides the expression for the fluid pressure after integrating with respect to \bar{z} and applying the outlet
 310 condition (13d),

$$\bar{p} = \frac{(1 - \bar{z}) I_0 \left(\sqrt{\frac{\phi}{Da}} \bar{R} \right)}{I_2 \left(\sqrt{\frac{\phi}{Da}} \bar{R} \right)}. \quad (36)$$

311 We compare the axial velocity profile (34) with the numerical solution in Fig. 5(a) as we vary the filter
 312 aspect ratio \bar{R} and find that the two solutions agree well. For smaller values of \bar{R} , a dependence of the
 313 axial velocity on depth \bar{z} emerges (Fig. 5b), which is consistent with the agreement in $\bar{v}(r)$ for larger
 314 values of \bar{R} (Fig. 5a). This indicates that Eq. (34) provides a good approximation to the flow for filters
 315 whose aspect ratio is not too small.

316 *5.2. Intra-particle dynamics*

317 An asset of our model is that, in addition to modelling the inter-particle dynamics, we also capture
 318 the intra-particle behaviour, which is difficult to observe experimentally. Studying the *As* concentration
 319 inside the particle, we find that, for particles at the inlet, $(\bar{r}, \bar{z}) = (0, 0)$, at the particle surface $\bar{r}_p = 1$,
 320 \bar{c}_p attains 1 almost immediately and remains at this value thereafter (Fig. 6a). However, at the exit,
 321 $(\bar{r}, \bar{z}) = (0, 1)$, the surface concentration (\bar{c}_p at $\bar{r} = 1$) takes a longer time to approach 1. Eventually, the
 322 intra-particle concentration reaches saturation, but this happens on a much longer timescale than the
 323 bulk removal timescale on which we have non-dimensionalised (Fig. 6c). This arises since contaminant is
 324 transported by advection and diffusion in the inter-particle space (with advection dominating since $Pe \gg$
 325 1) but occurs solely by diffusion in the intra-particle space. Thus, at the time we term breakthrough,
 326 when the inter-particle concentration reaches 1 everywhere in the liquid, the filter will still continue
 327 to adsorb arsenic, albeit at a much slower rate, until the intra-particle concentration also reaches 1
 328 everywhere in space.

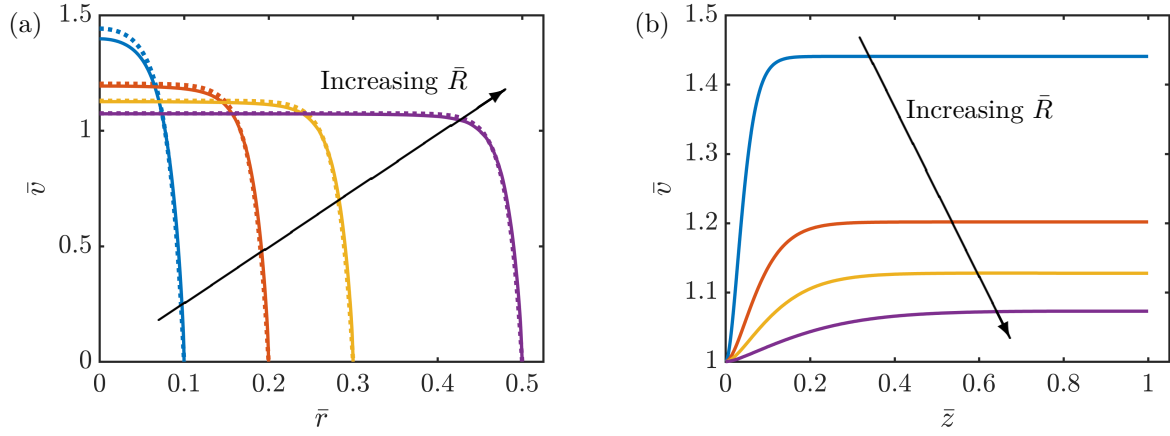


Figure 5: Profile of the fluid velocity \bar{v} as a function of (a) \bar{r} , at $\bar{z} = 1$ and (b) \bar{z} , at $\bar{r} = 0$, on increasing the aspect ratio, $\bar{R} = 0.1, 0.2, 0.3$ and 0.5 , in the direction of the arrow. The dotted curves in (a) represent the analytical solution corresponding to Eq. (34). The sample values of $\phi = 0.32$ (for a treated-laterite filter) and $L = 0.2$, and $Da = 10^{-4}$ for illustrative purposes, are used in the calculation. The values of the other parameters are listed in Tables 1 and 2.

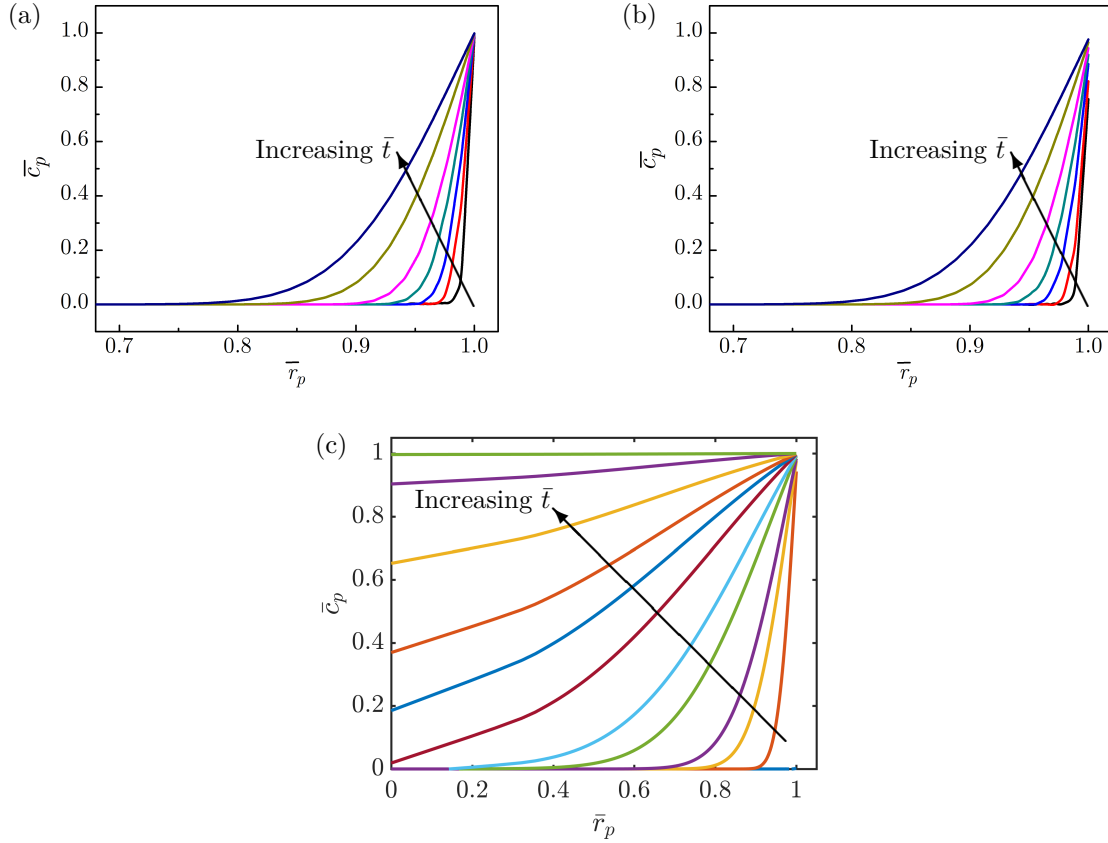


Figure 6: Profile of the intra-particle contaminant (*As*) concentration from Experiment 2, \bar{c}_p along the particle spherical coordinate with time \bar{t} at (a) $(\bar{r}, \bar{z}) = (0, 0)$ and (b) $(\bar{r}, \bar{z}) = (0, 1)$. The arrow indicate the profiles with increasing time, $\bar{t} = 0.01, 0.02, 0.05, 0.1, 0.2, 0.5$ and 1.0 . The plot in (c) shows the long-time dynamics inside the particle for $\bar{t} = 0.2, 1, 2, 6, 10, 20, 30, 40, 60, 100, 200$ (in the direction of the arrow), at $(\bar{r}, \bar{z}) = (0, 0)$. The values of the parameters used correspond to the lab-scale filter, as listed in Tables 1 and 2.

329 *5.3. Dependence on filter lifetime on key parameters*

In this final section we use the model for its chief purpose, to determine the lifetime of a filter for a given requirement. The governing system of equations (10), (11), (19), (22) and (25), subject to the initial and boundary conditions (13), (18), (23) and (26) with the dimensionless relation (24) is described by nine dimensionless parameters: Da , ϕ , ϕ_p , Pe , \mathcal{A} , \mathcal{B} , Re_p , Sh , β_1 and β_2 . It would be an onerous task to study the dependence of the system on each of these parameters individually, but we can facilitate this analysis by recasting the problem in terms of the following parameters:

$$\mathcal{M} = \frac{M}{\pi R^2 \rho_p (1 - \phi) \left(\frac{a_p^3 \mu}{\rho_1 D_p} \right)^{1/3}}, \quad \mathcal{Q}_i = \frac{Q_i}{\pi R^2 \left(\frac{\mu D_p^2}{\rho_1 a_p^3} \right)}, \quad \mathcal{C}_f = \frac{c_f}{\left(\frac{\rho_1 D_p}{\mu} \right) q_m \rho_p}. \quad (37)$$

These dimensionless parameters encapsulate the dependence on the key variables of interest, namely mass of filter, throughput and feed contaminant concentration, respectively. Expressing the system in this way allows us to perform efficient parameter sweeps to determine how the filter behaviour will change when we vary these key parameters. The nine dimensionless parameters can then be expressed in terms of these three core parameters, along with material parameters that will be unchanged (or can be easily ascertained by experiments):

$$Da = \left(\frac{a_p^2 \mu^{2/3} \kappa}{\rho_1^{2/3} D_p^{2/3}} \right) \frac{1}{\mathcal{M}^2}, \quad Pe = \left(\frac{\mu^2 D_p}{\rho_1^2 D_1^3} \right)^{1/3} \mathcal{Q}_i \mathcal{M}, \quad \mathcal{A} = 3(1 - \phi) \frac{4 + \mathcal{Q}_i^{1/2}}{2\mathcal{Q}_i} \mathcal{M}, \quad \mathcal{B} = \frac{\mathcal{M}}{\mathcal{C}_f},$$

$$Sh = 2 + \frac{1}{2} \mathcal{Q}_i^{1/2}, \quad \beta_1 = \frac{k_1 a_p^2 q_m \rho_p}{D_p} \mathcal{Q}_i \mathcal{C}_f, \quad \beta_2 = k_2 a_p^2 \left(\frac{\mu^2}{\rho_1^2 D_p^5} \right)^{1/3} \mathcal{Q}_i^2, \quad (38)$$

330 while, ϕ and ϕ_p are material parameters.

331 The lifetime \bar{t}_1 of the filter is defined as the time at which $\bar{c}_{\text{avg}} c_f > 10 \mu\text{g/L}$, according to the WHO
 332 guidelines [21]. As expected, the lifetime of the filter decreases with increasing throughput because of
 333 the higher processing rate (Fig. 7a). However, it varies in both a nonlinear and non-power-law manner
 334 as a result of the coupled intra- and inter-particle dynamics, a trend that would be difficult to anticipate
 335 from experiments. Thus, this predicts that when doubling the filter flow rate, the lifetime falls by less
 336 than half, which may prove promising for upscaling. An increase in the mass of adsorbent increases
 337 the total adsorption capability of the filter and thus increases the lifetime (Fig. 7a). Increasing the
 338 feed concentration leads to a lower filter lifetime, but this can be countered by increasing the mass of
 339 adsorbent used (Fig. 7b). As with the relationship between filter lifetime and throughput, the dependence
 340 on concentration is both nonlinear and does not exhibit a power-law relationship. The lack of a linear
 341 relationship means that for higher concentrations the filter lifetime may be longer than naively expected.
 342 Finally, we observe that the lifetime of the filter falls with with feed concentration but this effect may
 343 be mitigated by reducing the flow rate (Fig. 7c).

344 In Fig. 8 we show iso-lifetime curves: if the concentration of contaminant in the feed were to change,
 345 then these curves show how the flow rate must change to achieve a particular lifetime (Fig. 8a) and
 346 the improvements that are garnered by increasing the filter size (Fig. 8b). Since in many situations the
 347 required flow rate is a fixed quantity one might use this information to determine how many filters should

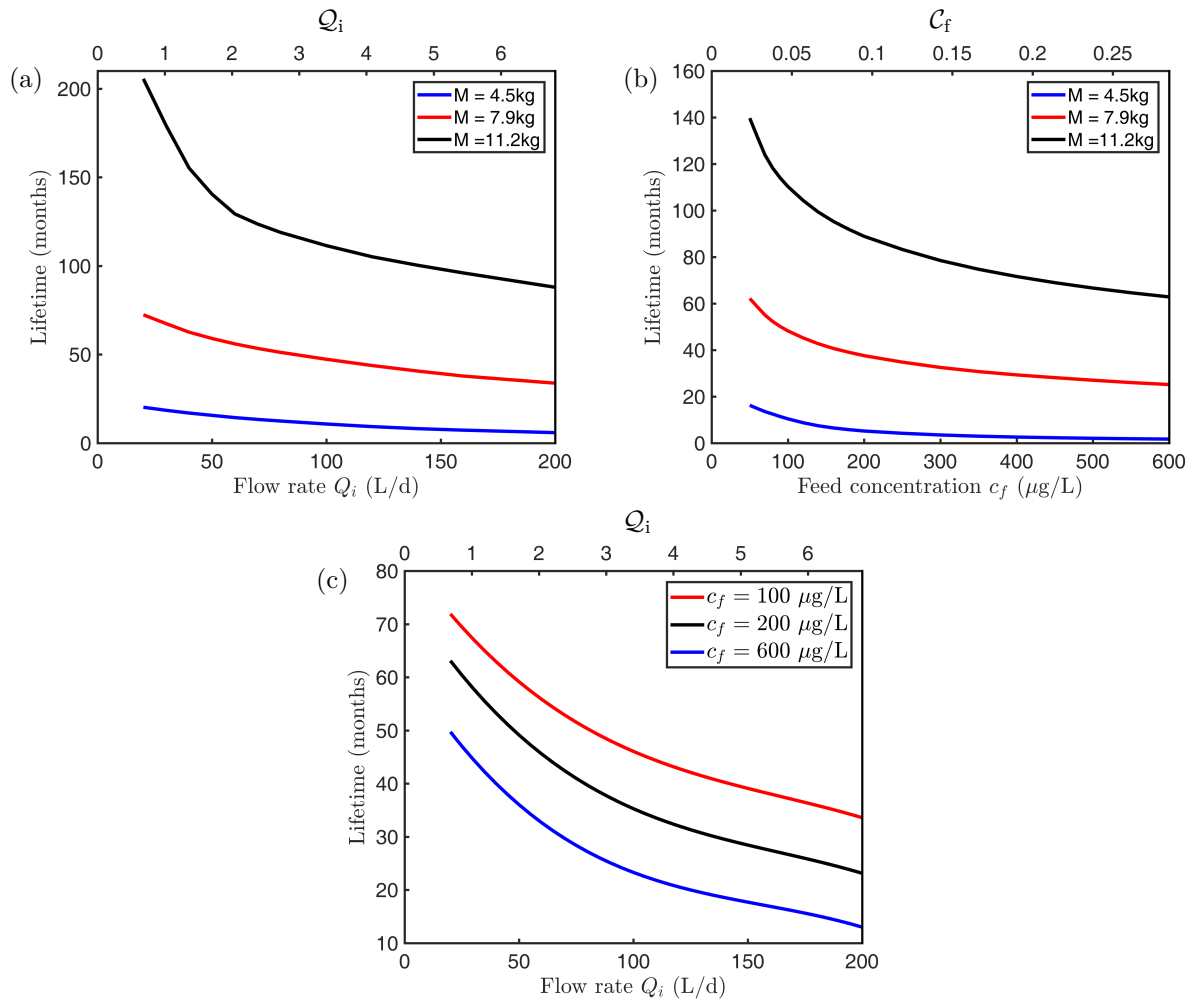


Figure 7: Variation of predicted lifetime of the filter for changes in (a) feed flow rate at different adsorbent dosage and fixed feed concentration, (b) feed concentration at different adsorbent dosage and fixed feed flow rate, and (c) feed flow rate with varying feed concentration at fixed adsorbent dosage. The values of the parameters considered here correspond to the field-scale filter, as listed in Table 3. On the lower x axis we show the dependence on real physical variables for $c_f = 100\ \mu\text{g/L}$, $Q_0 = 100\ \text{L/d}$, $R = 0.1\ \text{m}$ and $L = 0.35\ \text{m}$. On the upper x axis we show the dependence on the core dimensionless parameters defined in (37). The values of \mathcal{M} corresponding to the legends in (a) and (b) are 45, 79 and 112. The values of \mathcal{C} corresponding to the legend in (c) are 0.047, 0.095 and 0.285. While the dimensional scales apply to a single filtration device, the dimensionless scales enable predictions to be made for the filter lifetime for a range of field-scale filters.

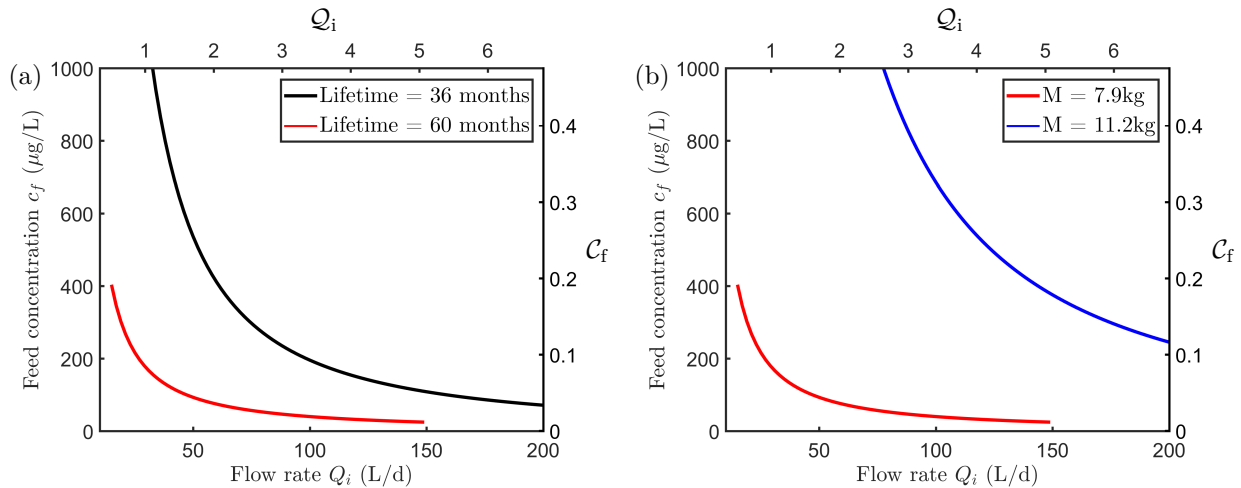


Figure 8: Iso-lifetime curves, along which the lifetime of the filter is constant, where filter lifetime is designated as the time when the output concentration exceeds $10 \mu \text{g/L}$. In (a) we present two different lifetimes, 36 and 60 months for a filter with $M = 7.9 \text{ kg}$ ($\mathcal{M} = 79$). In (b) we present two different filter masses, $M = 7.9 \text{ kg}$ ($\mathcal{M} = 79$) and $M = 11.2 \text{ kg}$ ($\mathcal{M} = 112$) corresponding to a lifetime of 60 months. The other values of the parameters considered here correspond to the field-scale filter, as listed in Table 3.

348 be run in parallel if they could only to be exchanged at set times due to restrictions on the frequency of
 349 maintenance visits.

350 For the utility of the filter from an end-user perspective, it is important to have a set of design-
 351 performance curves, which can provide the information on the desired lifetime as a function of the
 352 feed concentration, amount of adsorbent and the throughput. The information embedded within the
 353 graphs presented in Figs. 7 and 8 predicts the lifetime of a given filter, for example for a family home,
 354 and offer a method for determining how the filter should be modified to obtain the required lifetime
 355 under different operating conditions, such as upscaling to a school or community. This information can
 356 thus be used as a tool for the design of the filter for As , or indeed other adsorption-based, filtration,
 357 which can be modified according to a specific requirement.

6. Conclusions

No water-purification route is complete without the knowledge about its long-term behaviour, the safe operating lifetime, and the routes for controlling the characteristics of purified water. In this work we have shown how a model based on Langmuir kinetics can be used for the prediction of a fixed-bed adsorption column. Our model incorporates fluid transport, contaminant transport and adsorption on both the inter-particle and intra-particle scales. The fluid transport was modelled by the Darcy–Brinkman equation, and reaction–advection–diffusion equations to describe the inter-particle and intra-particle regions, to ultimately understand the adsorption behaviour of the contaminant in the filter. The intra-particle kinetic model was used for the first time for the prediction of filter lifetime.

Through non-dimensionalisation and proper identification of the system parameters, the set of partial differential equations was solved following finite-element schemes with specialised software. The simulation results were compared with simple experimental studies conducted for a single-bed column of raw laterite or treated laterite and values of the effective diffusion coefficients were determined. The resulting model was then free of any fitting parameters and was validated for a dual-bed column of raw and treated laterite. This model was further tested for different operating conditions (feed flow rate, contaminant concentration and filter height) and was proven to be effective in prediction of the system performance in those conditions.

The model was used to analyse the *As* transport and adsorption behaviour within the filter media, both on the inter- and intra-particle scales. This gave insight into the inherent multiscale behaviour of the filter that could not be extracted through the experimental measurement of bulk properties, which manifested itself through non-power law dependencies for the filter lifetime and multiple timescale behaviour.

Three core dimensionless system parameters were identified, which characterise the key variables in the *As* filter challenge: the required flow rate, the contaminant concentration, and the mass of laterite soil used. We showed how the model could predict the dependence of the filter lifetime on these core parameters. The filter lifetime vary significantly with these parameters, ranging from less than 10 months for small filters (4.5 kg) processing at high flow rates (200 L/d) or heavily contaminated ($\sim 500\mu\text{g/L}$) water, and over 100 months for larger filters (11.2 kg) processing water at lower flow rates ($< 50\text{ L/d}$) or lower contaminant concentrations ($100\mu\text{g/L}$). We extracted non-power-law trends that would be difficult to predict even qualitatively in the absence of the model and would take many years to obtain experimentally. We showed how the model analysis could be presented in the form of iso-lifetime curves, which allow for the simple prediction of filter design to achieve a given lifetime, and how a filter should be modified if, for example, the contaminant concentration or the required flow rate were to change.

While the model results were used to provide a set of characteristic curves that act as an assistive tool for the design of *As*-removal filters, the results readily generalise for the removal of other contaminants via adsorption-based filters. The core result of this work is the systematic reduction of a multiscale model to a set of characteristic curves which bypasses the need for infeasibly long experiments to provide quick and simple predictions for adsorption-based filters. We hope that this work may be adopted to assist in the future deployment and management of these arsenic filters.

397 **Acknowledgements**

398 The collaborative work between the two institutions was initiated by the Global Challenges Research
399 Fund. IMG gratefully acknowledges support from the Royal Society through a University Research
400 Fellowship. The authors acknowledge helpful discussions with Lucy Auton, Graham Baird and Doireann
401 O’Kiely. RM gratefully acknowledges support from the the Royal Society through a Challenge Grant.
402 SM gratefully acknowledges support from the Royal Society and EPSRC. The group from the Indian
403 Institute of Technology Kharagpur gratefully acknowledges the inter-disciplinary collaborative initiative
404 taken up by the Mathematical Institute at the University of Oxford.

406 **Nomenclature**

407

408 (r, z) cylindrical coordinates, m409 \mathcal{A} $3k_f(1 - \phi)L/v_i a_p$ 410 \mathcal{B} $\rho_p \nu^2 q_m / c_f L^2$ 411 \mathcal{C}_f dimensionless measure of contaminant concentration412 \mathcal{M} dimensionless measure of filter mass413 \mathcal{Q}_i dimensionless measure of volumetric flow rate414 \mathcal{R}^2 linear regression coefficient415 A cross-sectional area of filter, m^2 416 a_p particle radius, m417 c contaminant concentration, kgm^{-3} 418 c_0 initial arsenic concentration in experiment, kgm^{-3} 419 c_e initial arsenic concentration in experiment, kgm^{-3} 420 c_f contaminant feed concentration, kgm^{-3} 421 c_p contaminant concentration at the particle surface, kgm^{-3} 422 D_1 effective diffusion coefficient of contaminant in porous bed, m^2s^{-1} 423 D_p diffusion coefficient of contaminant inside particle, m^2s^{-1} 424 Da Darcy number425 K_0 adsorption equilibrium constant, m^3kg^{-1} 426 k_1 adsorption rate, $m^3kg^{-1}s^{-1}$ 427 k_2 desorption rate, s^{-1} 428 k_f mass-transfer coefficient, ms^{-1} 429 L filter length, m430 M mass of adsorbent, kg431 p fluid pressure, Pa

432	p_a	ambient pressure, Pa
433	Pe	Péclet number
434	Q	experimental volumetric flow rate, m^3s^{-1}
435	q	adsorption capacity, kg/kg
436	Q_i	volumetric inlet flux, m^3s^{-1}
437	q_m	maximum amount of contaminant that can be adsorbed, kg/kg
438	R	filter radius, m
439	r_p	particle radial coordinate, m
440	Re	Reynolds number
441	Re_p	particle Reynolds number
442	Sc_p	Schmidt number
443	Sh	Sherwood number
444	t	time, s
445	\mathbf{u}	fluid velocity in cylindrical coordinates ($=u,v$), ms^{-1}
446	v_i	inflow velocity, ms^{-1}
447	V	volume of synthetic solution used in experiment, m^3
448	Greek symbols	
449	α	$\phi D_p / D_1$
450	β_1	dimensionless adsorption rate
451	β_2	dimensionless desorption rate
452	Δp	pressure difference in experiment, Pa
453	κ	permeability of the porous medium, m^2
454	μ	dynamic fluid viscosity, Pa s
455	ϕ	porosity of the porous medium
456	ξ	surface area factor exposed to free fluid, m^{-1}

457 **References**

- 458 [1] H. N. Tran, S.-J. You, A. Hosseini-Bandegharaei, and H.-P. Chao. Mistakes and inconsistencies
459 regarding adsorption of contaminants from aqueous solutions: a critical review. *Water Research*,
460 120:88–116, 2017.
- 461 [2] M. Leist, R. J. Casey, and D. Caridi. The management of arsenic wastes: problems and prospects.
462 *J. Haz. Mat.*, 76(1):125–138, 2000.
- 463 [3] J. C. Ng, J. Wang, and A. Shraim. A global health problem caused by arsenic from natural sources.
464 *Chemosphere*, 52(9):1353–1359, 2003.
- 465 [4] I. A. Katsoyiannis and A. I. Zouboulis. Removal of arsenic from contaminated water sources by
466 sorption onto iron-oxide-coated polymeric materials. *Water research*, 36(20):5141–5155, 2002.
- 467 [5] WHO reports. Arsenic proposed drinking water regulation: A science advisory board
468 review of certain elements of the proposal. *US EPA*, EPA-SAB-DWC 1-001, 2000,
469 <https://nepis.epa.gov/exe/zypurl.cgi?dockey=p100ff7r.txt>.
- 470 [6] A. Maiti, S. DasGupta, J. K. Basu, and S. De. Batch and column study: adsorption of arsenate
471 using untreated laterite as adsorbent. *Industrial & Engineering Chemistry Research*, 47(5):1620–
472 1629, 2008.
- 473 [7] A. Maiti, H. Sharma, J. Kumar Basu, and S. De. Modeling of arsenic adsorption kinetics of synthetic
474 and contaminated groundwater on natural laterite. *J. Haz. Mat.*, 172(2–3):928–934, 2009.
- 475 [8] A. Maiti, J. K. Basu, and S. De. Experimental and kinetic modeling of as (v) and as (iii) adsorption
476 on treated laterite using synthetic and contaminated groundwater: Effects of phosphate, silicate
477 and carbonate ions. *Chem. Eng. J.*, 191:1–12, 2012.
- 478 [9] S. K. Maji, A. Pal, T. Pal, and A. Adak. Sorption kinetics of arsenic on laterite soil in aqueous
479 medium. *J. Environ. Sci. and Health, Part A*, 42(7):989–996, 2007.
- 480 [10] G. S. Bohart and E. Q. Adams. Some aspects of the behavior of charcoal with respect to chlorine.
481 *J. American Chem. Soc.*, 42(3):523–544, 1920.
- 482 [11] A. Wolborska. Adsorption on activated carbon of p-nitrophenol from aqueous solution. *Water*
483 *Research*, 23(1):85–91, 1989.
- 484 [12] S. Mondal, A. Roy, R. Mukherjee, M. Mondal, S. Karmakar, S. Chatterjee, M. Mukherjee, S. Bhat-
485 tacharjee, and S. De. A socio-economic study along with impact assessment for laterite based
486 technology demonstration for arsenic mitigation. *Science of The Total Environment*, 583:142–152,
487 2017.
- 488 [13] K. Tsiberkin. Effect of inertial terms on fluid–porous medium flow coupling. *Transport in Porous*
489 *Media*, 121(1):109–120, 2018.

- 490 [14] J. M. Coulson, J. F. Richardson, J. R. Backhurst, and J. H. Harker. *Chemical Engineering Vol 2*.
491 Pergamon Press, Oxford, 1968.
- 492 [15] Y. Liu and L. Shen. From langmuir kinetics to first-and second-order rate equations for adsorption.
493 *Langmuir*, 24(20):11625–11630, 2008.
- 494 [16] J. M. Coulson, J. Francis Richardson, J. R. Backhurst, and J. H. Harker. *Chemical Engineering Vol*
495 *1*. Pergamon Press, Oxford, 1968.
- 496 [17] F. H. Garner and R. B. Keey. Mass-transfer from single solid spheres—I: Transfer at low reynolds
497 numbers. *Chem. Eng. Sci.*, 9(2–3):119–129, 1958.
- 498 [18] B. S. Persons. *Laterite: Genesis, Location, Use*. Springer Science & Business Media, 2012.
- 499 [19] M. Lunt. Introduction to statistical modelling: linear regression. *Rheumatology*, 54(7):1137–1140,
500 2013.
- 501 [20] S. Gupta and B. V. Babu. Modeling, simulation, and experimental validation for continuous
502 Cr (VI) removal from aqueous solutions using sawdust as an adsorbent. *Bioresource Technology*,
503 100(23):5633–5640, 2009.
- 504 [21] WHO Chronicle. Guidelines for drinking-water quality, fourth edition. 38(4):104–8, 2011.

Supplementary Information

Kinetic experiments

The kinetic experiments were carried out by measuring the concentration of the solution at different instants of time. For this, nine conical flasks each having 100 ml of feed (aqueous solution of arsenic of known concentration) were taken and known weight of adsorbent was added into that. These flasks were then maintained under continuous shaking (speed 150 rpm, temperature 25°C). Each flask was removed at different time points and samples were analyzed for arsenic concentration. This concentration was used to calculate the adsorption capacity (q) at that instant of time. The q values were thus calculated at nine time points and used to calculate the kinetic constants using Eq. (31). A plot of c/c_0 (where c_0 is the initial concentration) with time for RL and TL is shown in Figure S1.

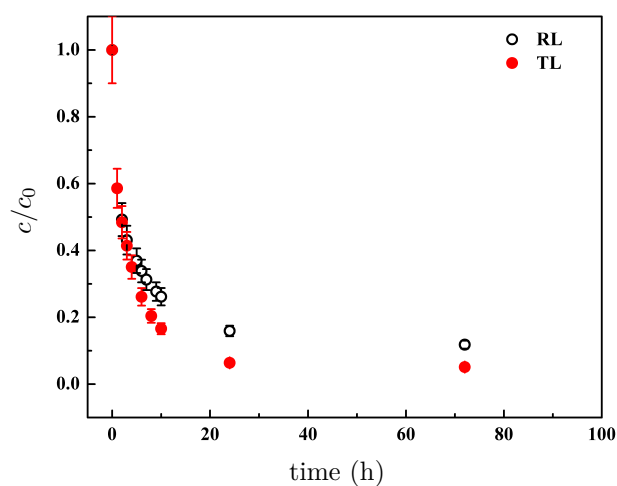


Figure S1: Plot of c/c_0 with time for RL and TL during kinetic study.